3 Experimental Methods

The experimental methods used in this study span from combustor design to spectroscopy. Tunable Diode Laser Absorption Spectroscopy (TDLAS) is used to obtain a dynamic measurement of product gas temperature. Equivalence ratio fluctuations are measured via the absorption of an infrared Helium-Neon laser. Hydroxyl radical (OH*) chemiluminescence is used as an indicator of chemical reaction rate. Velocity fluctuations are measured using the two-microphone method. The methods used in this investigation are described in this chapter.

3.1. Dynamic Temperature Measurement

A time-resolved measurement of gas temperature was achieved using Tunable Diode Laser Absorption Spectroscopy. The transitions used in this study are described, as well as the methodology for using TDLAS to measure flame dynamics.

3.1.1. Near-IR Line Candidates. The transitions of water vapor in the infrared region are shown in Figure 3.1 [1]. The absorption features overlap the wavelengths of available semiconductor lasers in many places. The choice of the particular wavelengths used in this study was a product of several factors. For a transition to be attractive with respect to spectroscopy, it must exhibit isolation from other absorbing species. The linestrength must be intense enough to insure adequate absorption. Since temperature will be calculated from these measurements in particular, temperature sensitivity, and thus lower-state energy, is also a consideration.

The parameters available in the HITRAN spectroscopic database [2] were used to simulate the transitions of water vapor. From Figure 3.1, it can be seen that the 1.4 μm and 1.8 μm region are attractive. At 2000K, two of the strongest transitions are at 1.392 μm (7185.59 cm^{-1}) and 1.343 μm (7444.37 cm^{-1}), as seen in Figure 3.2. The temperature sensitivities of the transitions are shown in Figure 3.3. As stated in Section 1.3.2, an almost infinite number of transitions contribute to the absorption at one

wavelength, a product of the hundreds of species in a combustion environment, each with a multitude of transitions. In this study, wavelengths were chosen that were dominated by several strong transitions within one cm^{-1} from the laser frequency. Appendix B1.2 shows the spectroscopic data that was used to simulate the transitions used in this study.

Using the information from Figure 3.3, a polynomial was fit to describe how the ratio of the linestrengths varies with temperature, in the form

$$T[K] = 7536.5054R^4 - 22764.2232R^3 + 27500.227R^2 - 13752.802R + 3254.5524 \quad (3.1)$$

Where T is temperature [K] and R is the ratio of the peak spectral absorption coefficient at 7444.37 cm-1 to the peak spectral absorption coefficient at 7185.59 cm-1. Equation 3.1 was then used to correlate the experimental absorption coefficients to gas temperature.

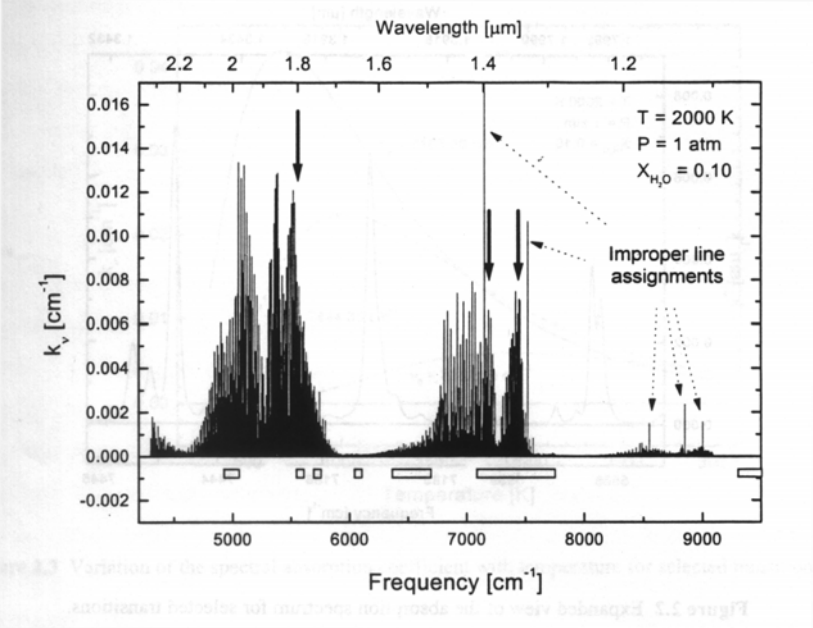

Figure 3.1. Water Absorption Spectra. Calculated absorption spectrum of water at 2000K overlaid with available diode laser wavelengths (gray bars). The heavy arrows indicate candidate transitions [1].

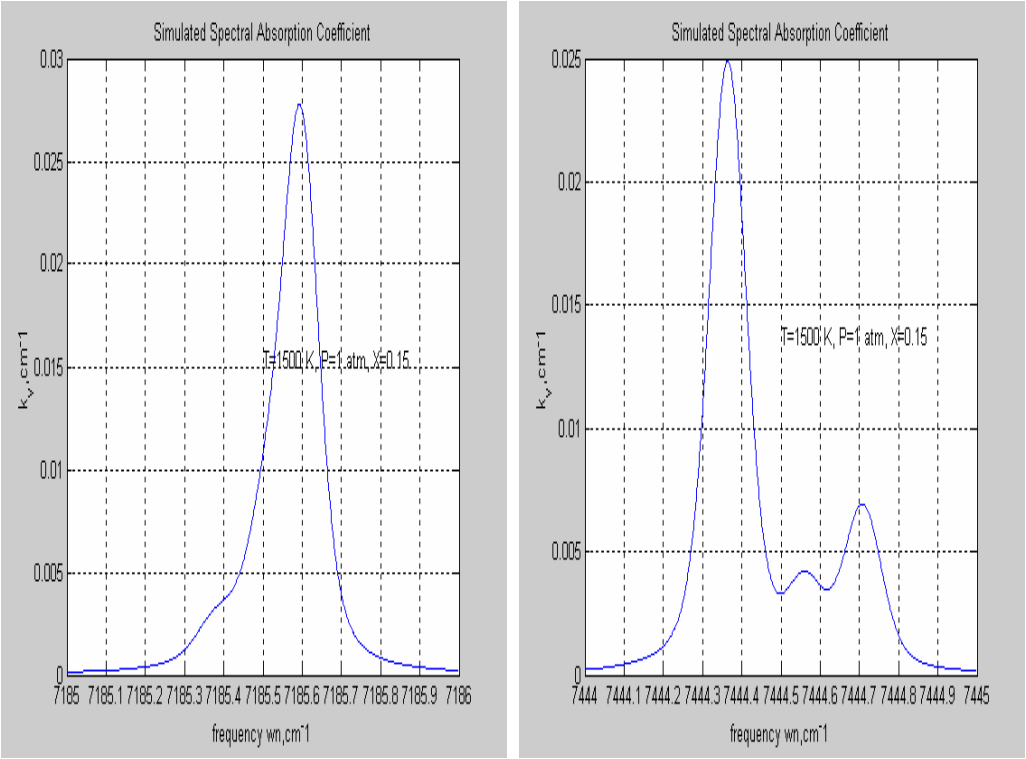

Figure 3.2. Selected Transitions. Expanded view of transitions used in this study.

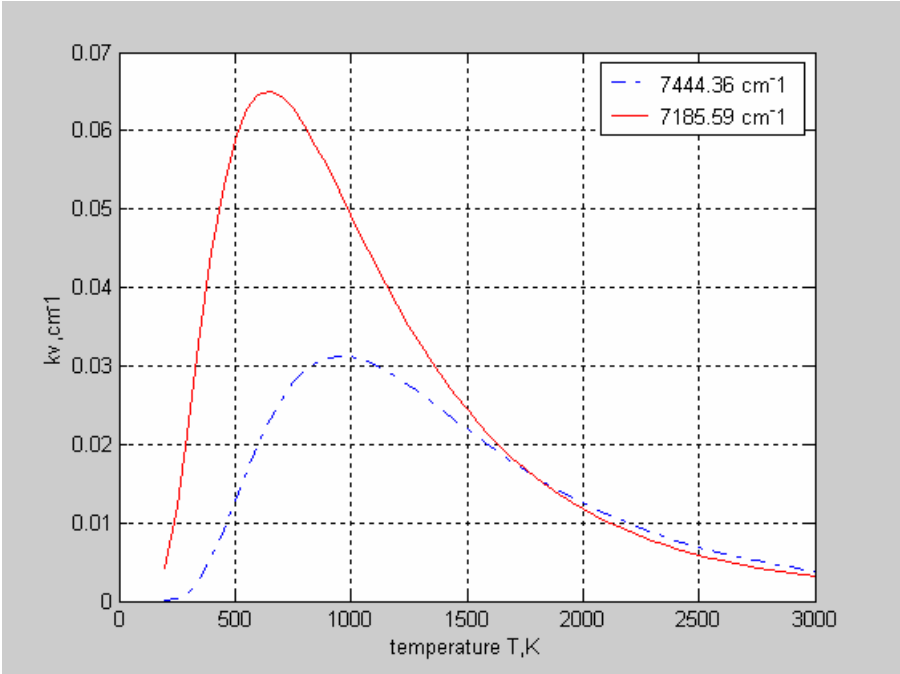

Figure 3.3. Temperature Dependence. The dependence of linestrength on temperature.

3.1.2 Measurement Sensitivity. The measurement sensitivity of a spectroscopic measurement is the product of many factors. Systematic errors arise from uncertainties in spectroscopic parameters, flow-field non-uniformities, and errors in the baseline determination. Beam-steering, emissions, laser noise, and detector noise result in random errors.

To calculate properties from spectroscopic data; the strengths, positions, broadening, and shift parameters of individual transitions are needed. The spectroscopic parameters used in this study were taken from the HITRAN/HITEMP 2000 general database [2]. Typically, only transitions strong at room temperature have been measured (within 2%), while high temperature transitions are often calculated. When measured at room temperature, high temperature transitions are accurate to approximately 20% [1]. Broadening and shift parameters often must be calculated. Fortunately, the parameters for transitions used in this study are well known.

Since tabulated linestrengths and positions are often more accurate than broadening parameters, the ratio of integrated lineshapes, R , is often used in temperature measurement. However, if the transitions used are well known, the ratio of peak absorbances, R_ν , can be used, as was done in this study. The disadvantage to using R_ν is that the different broadening characteristics of the transitions used are not taken in to account. The lineshape dependence is usually similar for the two transitions, so chances in pressure and concentration do not present significant errors. As shown in Figure 3.4, a change in concentration of 23% only changes the temperature by 4%.

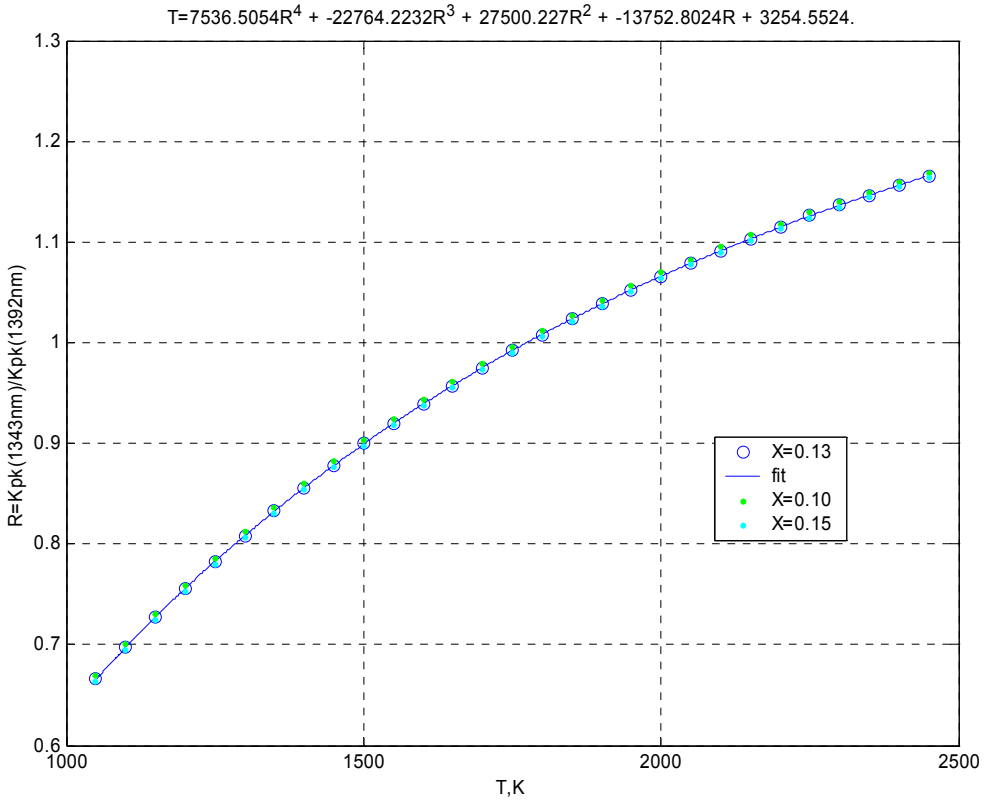

Figure 3.4. Sensitivity to Concentration. A change in concentration does not significantly change R.

Since the spectroscopic parameters are well known in this study, the dominant source of systematic error is flowfield non-uniformity. Absorption is a line-of-sight measurement, i.e. effects are integrated along the path length of the laser beam. Therefore, non-uniformities along the path length cannot be accurately resolved without resorting to tomography. Care was taken to perform the measurement at a location where the flow was relatively uniform. However, non-uniformities along the path length presented some trouble in interpreting the data (see Section 4.3.4). In past experiments on a forced-vortex burner, the 1343/1392 nm line pair was shown to under-predict the true path-averaged temperature by less than 10% [1].

Random error can also enter spectroscopic measurements in a variety of ways. Beam-steering caused by fluctuations in the temperature field can misalign the lasers. In the same way a pencil seems to bend when placed in the water, laser beams bend in the

presence of density gradients. Beam-steering effects were combated by frequent realignment of the lasers, the baseline determination technique, and focusing optics in front of the detectors. Emissions from other light sources that radiate in the infrared can interfere with the laser signal. The photodiode detectors were placed inside a dark box, with only a small aperture to allow the laser beam to pass. Care was taken to position the detectors facing away from the flame. Noise from the lasers and detectors also effects the measurement. Random errors were minimized by using polynomial baselines (Appendix B2) and digitally filtering the data at the frequency of interest (see Procedures).

3.1.3 Experimental Hardware. The experimental setup for TDLAS includes the diode lasers, controllers, optics, and detectors as shown in Figure 3.5. The semiconductor distributed feedback diode lasers, one at 1343 nm and one at 1392 nm, were obtained from Laser Components GmbH, Inc. They have a nominal power of 5 mW and can be tuned with respect to wavelength and power depending on case temperature and injection current. The lasers are mounted in diode mounts (ILX Lightwave LDM-4407) with thermo-electric coolers (TEC) to control the case temperature. A laser diode controller (ILX Lightwave LDC-3908, LDC-3916370 modules) is used to set temperature and injection current. The controller allows the injection current to be modulated via an external connection to a function generator. A laser diode beam is very diffuse, so off-axis paraboloidal reflectors (Melles-Griot) or aspheric lenses (New Focus 5723-H-C) are used to collimate the beam. The beam is directed across the flame, where a flat mirror reflects the beam back across the flame to the optical table. Another flat mirror (Newport 05D20ER.2-PF) directs the beam through a 2" focusing lens (Thorlabs LB1917-C) and onto a InGaAs photodiode detector (Thorlabs FGA10). The circuit diagram for the detector is shown in Appendix E. The circuit converts the current signal from the photodiode to a voltage signal and provides amplification. The bandwidth of the circuit is 10kHz.

The absorption of two transitions, and thus two lasers, is required for the temperature measurement. To insure accuracy, the beams must travel on approximately the same path. The beams are aligned to intersect in the measurement volume as seen in Figure 3.6, so that the minimum distance occurred in the crucial path length. Care is

taken to keep the total path length (from laser to detector) approximately equal for the two beams. The actual configurations for the laminar and turbulent combustors are shown in Figures 3.7 and 3.8, respectively.

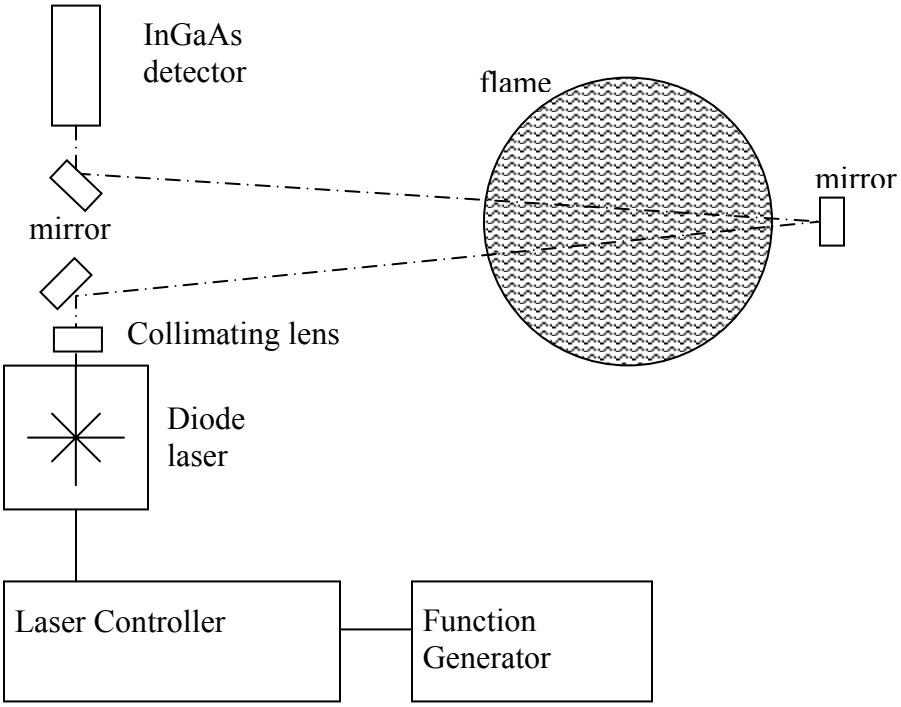

Figure 3.5. Diode-Laser Experimental Setup. The beams (only one shown) pass through the flame twice to increase signal to noise ratio.

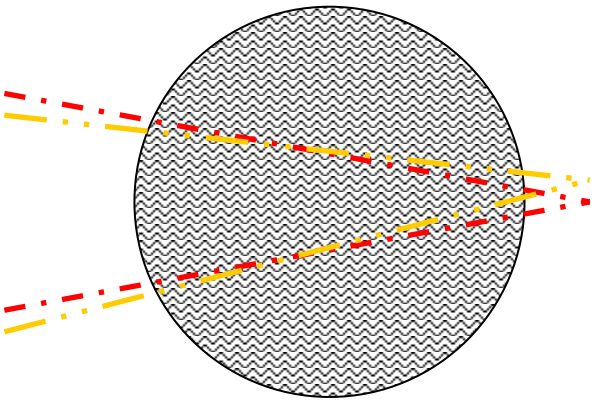

Figure 3.6. Beam Paths. The beams are on approximately the same path.

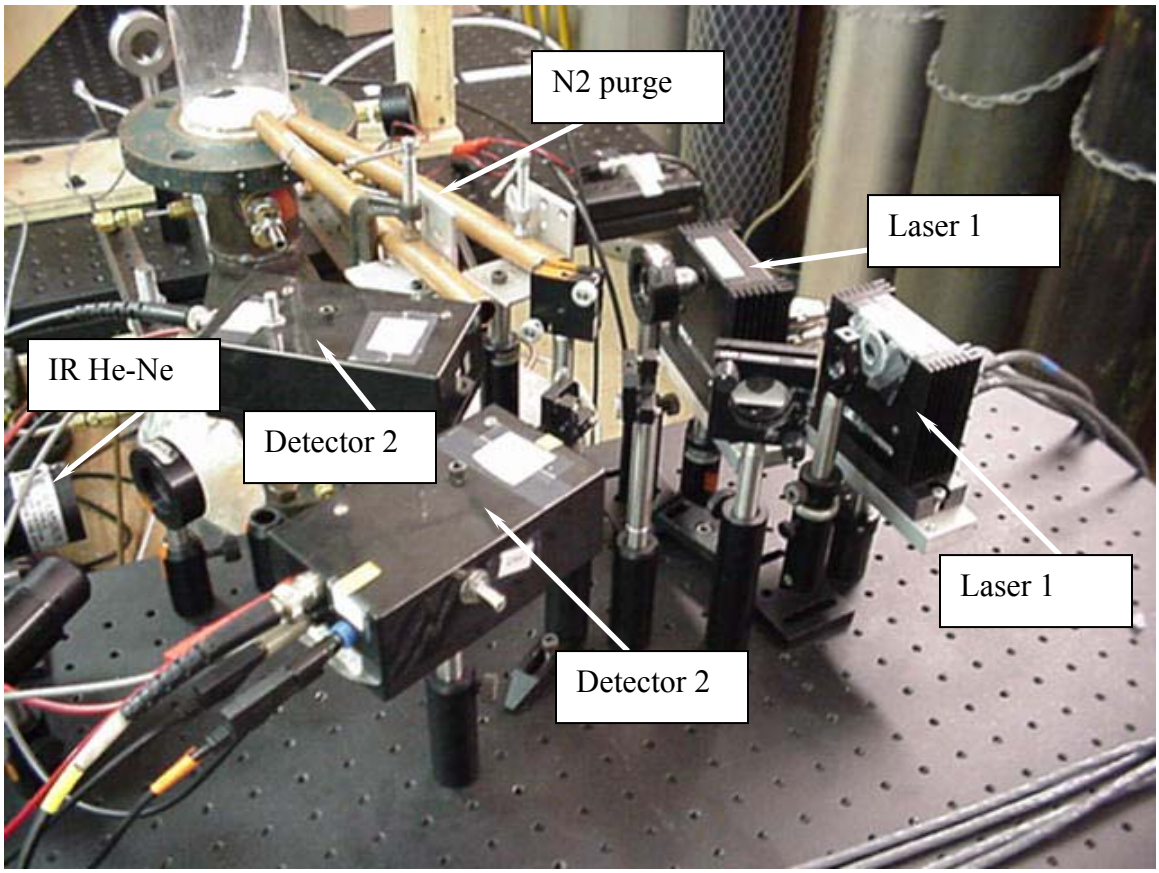

Figure 3.7. Laminar Burner Setup. The lasers and detectors were kept on the same optical bench: 1-1343nm, 2-1392nm.

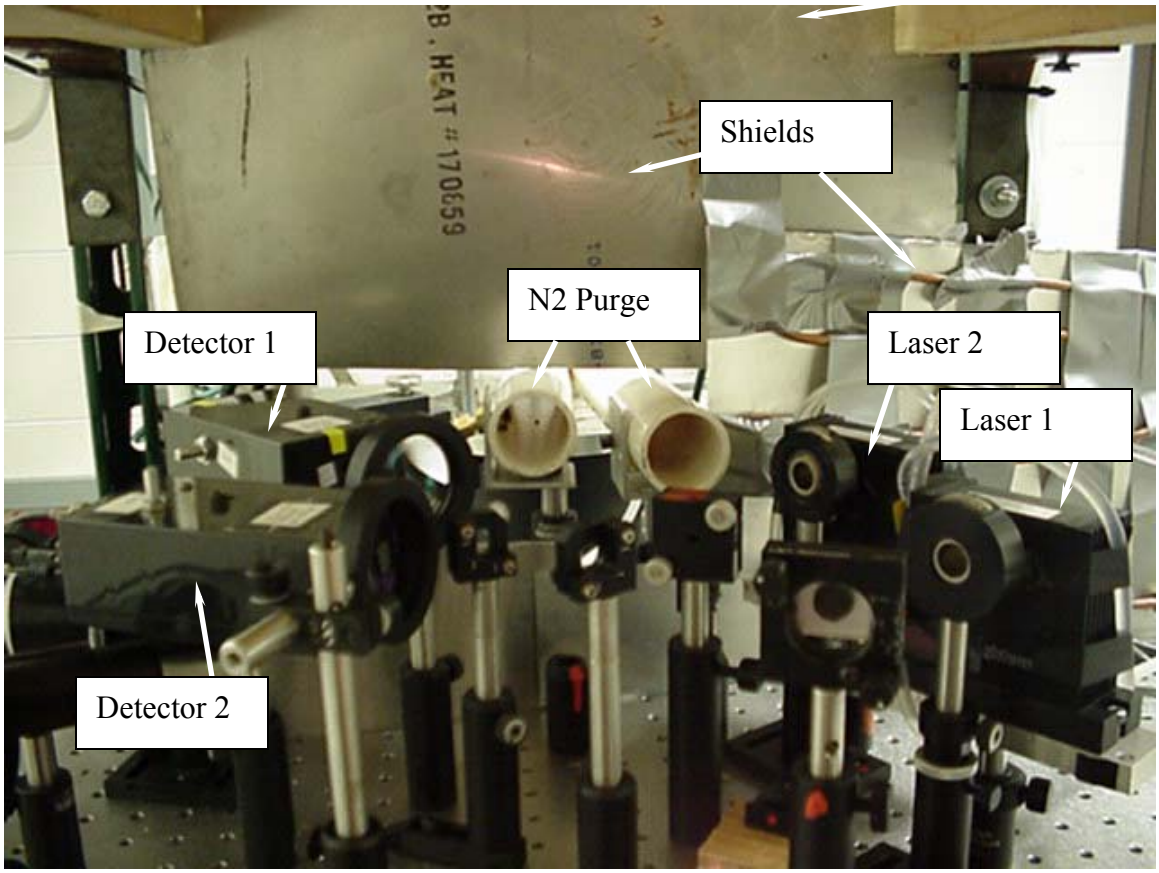

Figure 3.8. Turbulent Burner Setup. Water-cooling and shields protect the optics from the flame.

3.1.4. Procedure. A procedure was developed to obtain accurate dynamic measurements of gas temperature.

1. Align Optics: The diode laser optics must be aligned to insure accurate absorption data. First, the parabolic mirror or aspheric lens must be adjusted to collimate the beams. The aspheric lenses used in this study provided a reasonably collimated beam with a diameter of approximately 3-5 mm. Once adequate collimation is achieved, the beams are directed along the paths shown in Figure 3.5. Working from laser to detector, the mirrors are adjusted to align the beam on the desired path and center the beam on the detectors. Often when first positioning optical components, a visible He-Ne laser was placed at the detector location. In this manner, all optics could be aligned using the visible laser. Then, the beam from the diode laser was aligned to follow the same path as the visible beam. Care must be taken to keep the beam path parallel (at the same axial

coordinate with respect to the burner) along the path length. The detector gain is then adjusted to an output voltage of 2-4 Vdc. Optical noise may infiltrate the detector signal as a result of etalon effects (reflections of the various optical components feeding back to the detector). This noise source can be remedied by making small adjustments to the beam path.

2. Ambient Air Absorption: The absorption from ambient air (humidity) must be measured to correct the flame absorption measurements. Although the majority of the path length outside of the measurement volume is purged with nitrogen, significant absorption from ambient air is still present. With the nitrogen purge on and dry air flowing through the measurement volume, a wavelength-scanning technique (see Appendix B2) is used to measure the absorption resulting from humidity in the ambient air.

3. Flame Absorption: After the flame has reached steady-state, the lasers must be realigned to adjust for beam-steering effects of the flame (density gradients deflect the beam the same way water bends light). Then, a wavelength-scanning technique is used to measure the mean absorption from the flame. The data is also used to solve for the reference intensity of the dynamic data. For the dynamic (time-resolved) data, a direct absorption method is used, i.e. the lasers are maintained at the linecenters of the transitions that they are probing. The desired frequency resolution (1.5 kHz) and the speed of the data acquisition system (8 channels at 3 kHz) prohibited using a wavelength-scanning technique for the dynamic data. For the turbulent data, mean absorption data was collected at each modulation frequency using the wavelength-scanning technique. Due to the steady nature of the laminar flame, mean absorption data was only recorded at the beginning and end of each test.

4. Data Post-Processing: The mean data from the wavelength-scanning technique and the direct absorption data are used to obtain a high-bandwidth measurement of gas temperature. First, the wavelength-scanning data is used to find the reference intensities and steady-state gas temperature as detailed in Appendix B2. To obtain accurate temperature data, the absorption data is corrected with respect to the ambient air as shown in equation 3.2

$$K_{flame} = K_{total} - K_{air} \tag{3.2}$$

where K_{flame} is the absorption used in the temperature calculation, total refers to the uncorrected data, and air refers to the absorption due to the ambient air. Figure 3.9 shows typical absorption lineshapes in the ambient air. Figure 3.10 shows typical absorption lineshapes of the flame that have not yet been corrected.

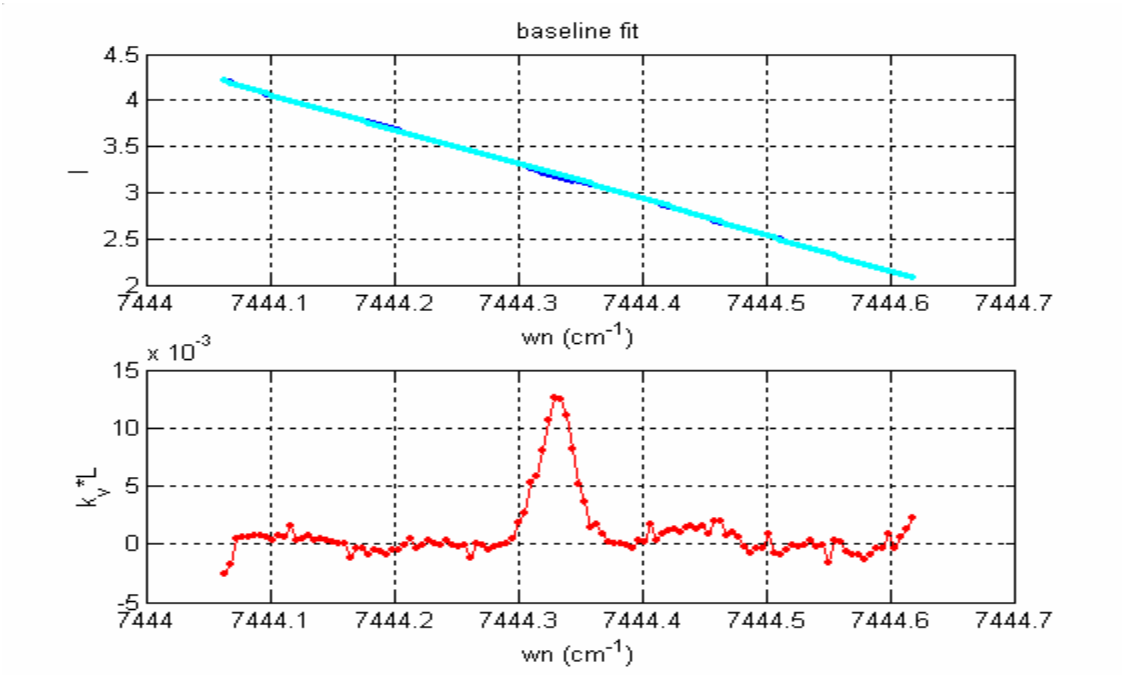

(a)

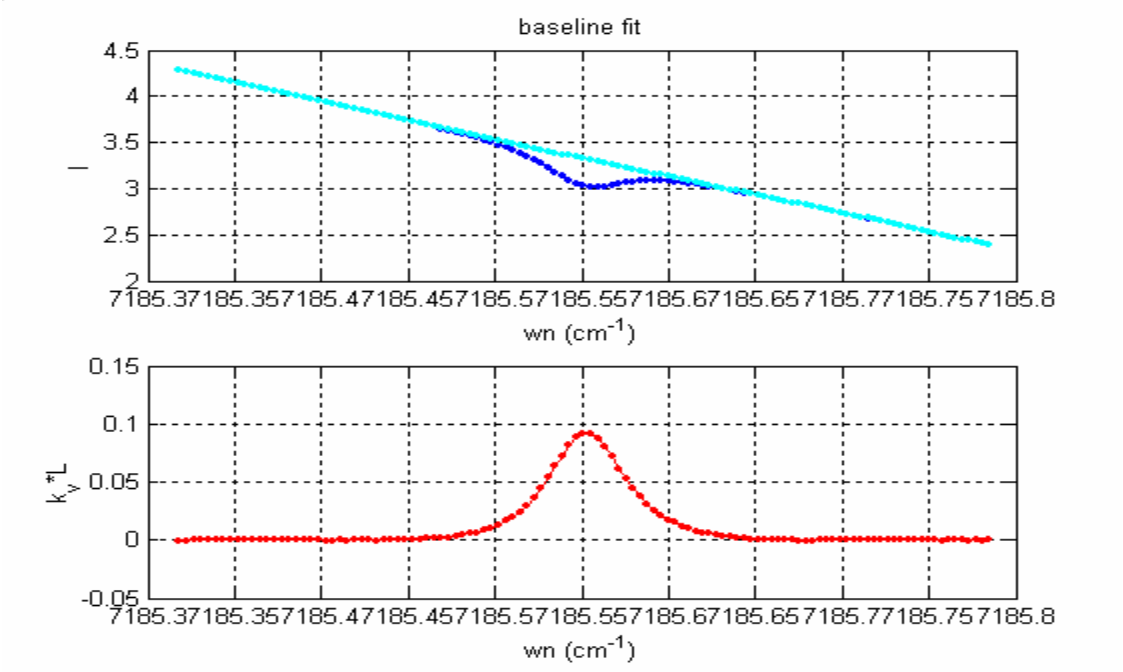

(b)

Figure 3.9. Absorption Lineshapes in Ambient Air. The absorption of water in ambient air must be accounted for to obtain accurate temperatures (a) 7444.37 cm^{-1} (b) 7185.59 cm^{-1}.

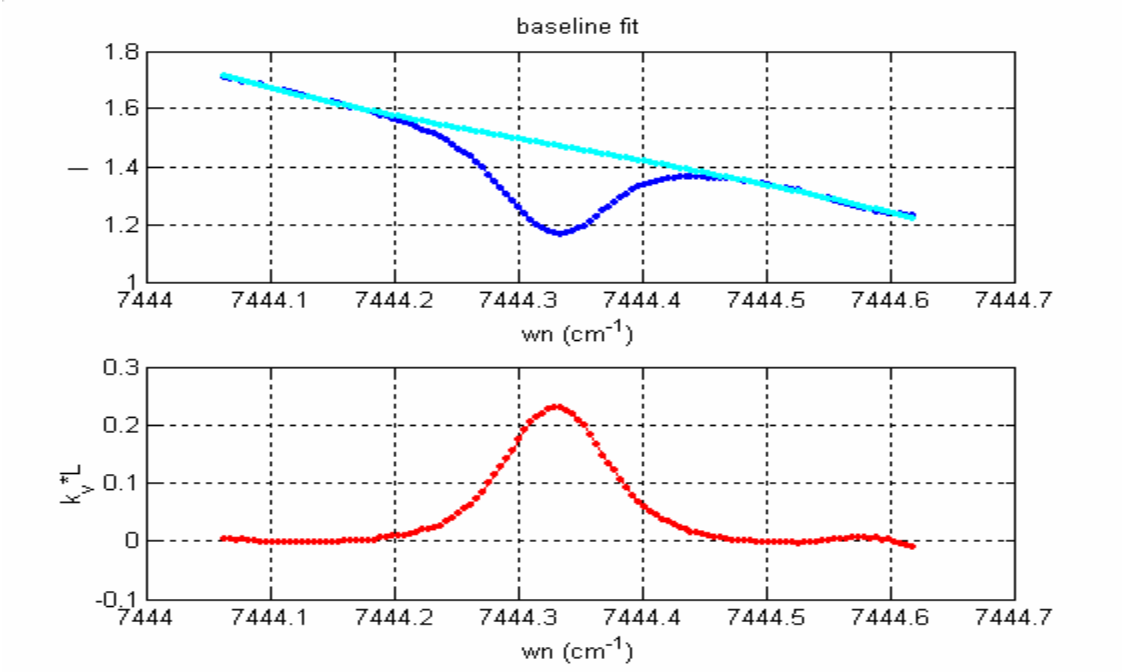

(a)

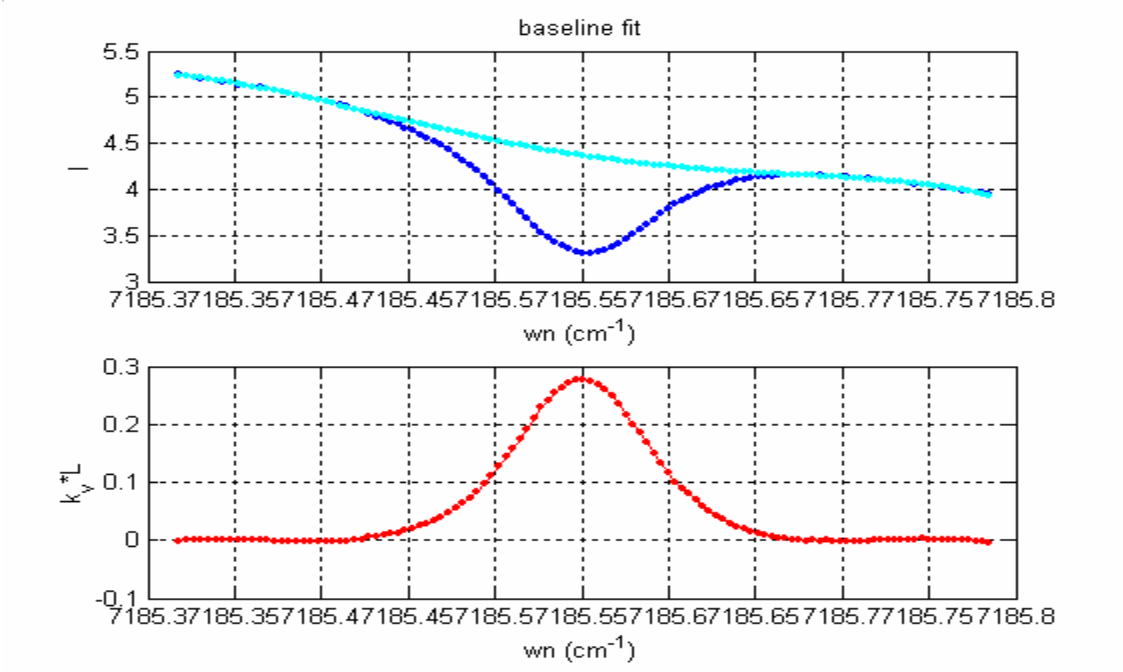

(b)

Figure 3.10. Absorption Lineshapes with Flame. The water absorption in the presence of the flame is much greater than the background absorption.

The direct absorption data suffers low-frequency modulation due to beam steering and flow discontinuities. These effects are countered by applying a 2000th order Finite Impulse Response (FIR) digital bandpass filter to the data at the excitation frequency (frequency at which the flame was acoustically forced). The filter is applied so as not to affect the phase of the signal, as seen in Figure 3.11. The mean is then added back to the filtered signal. The resulting signal is taken as the intensity *I*. The reference intensity, *Io*, is solved for using the lineshape data through equation 3.3

$$I_0 = \frac{\bar{I}}{\exp\left(-\left(K_{tot,o} + K_{air}\right)\right)} \tag{3.3}$$

where $\bar{I}$ is the mean intensity, $K_{tot,o}$ is the uncorrected absorption from the wavelength-scanning measurement, and K_{air} is the absorption from the ambient water. For the laminar data, the same reference intensity is used throughout the data set. In the turbulent case, the reference intensity was solved for at each excitation frequency. The temperature is computed at each time step by substituting the ratio of the absorbances of

the two transitions, R, into equation 3.1. A spectrum analysis is then calculated on the resulting time trace data to obtain power spectral densities and frequency response functions. All post-processing is completed using Matlab ®.

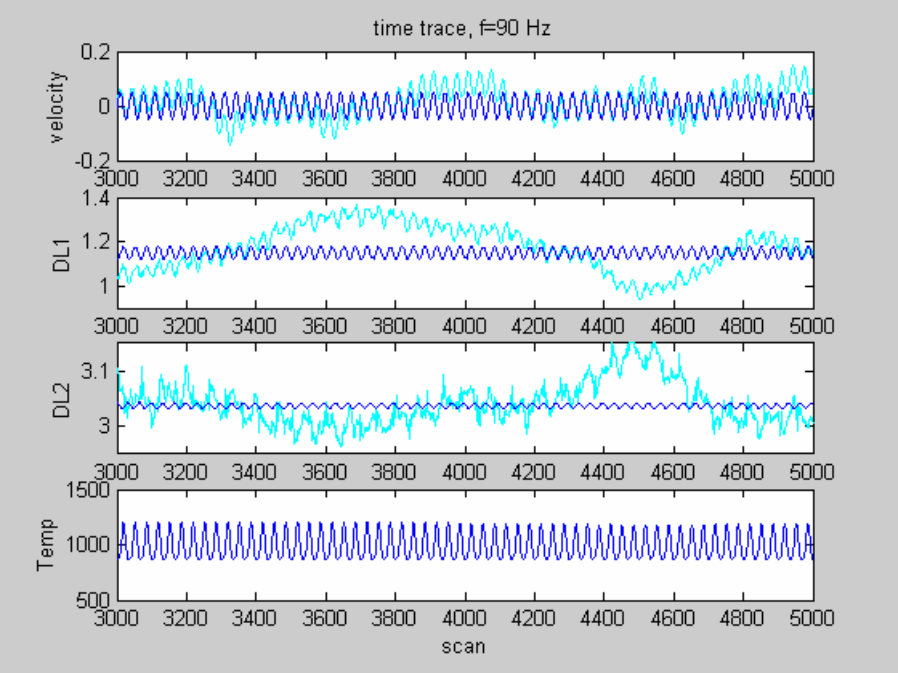

Figure 3.11. Digital filter. The digital filter does not affect the phase of the data.

3.2 Equivalence Ratio Fluctuations

Equivalence ratio fluctuations were measured upstream of the flame through methane absorption. An infrared He-Ne laser with emission at 3392 nm was used.

3.2.1. IR Line Candidates. The infrared Helium-Neon laser determined the transition probed for equivalence ratio fluctuation measurements. A strong methane transition overlaps with the emission of an IR He-Ne laser at 3.39 μm. Since the He-Ne laser cannot be wavelength-tuned, this transition must be used. As seen in Figure 3.12, the methane transition is very strong. Although this allows measurement of very low concentrations of methane, it severely limits the pathlength at higher concentrations. For

combustion experiments, with methane concentrations from 4% - 10%, the pathlength was limited to approximately 4 cm to maintain adequate signal to noise ratios.

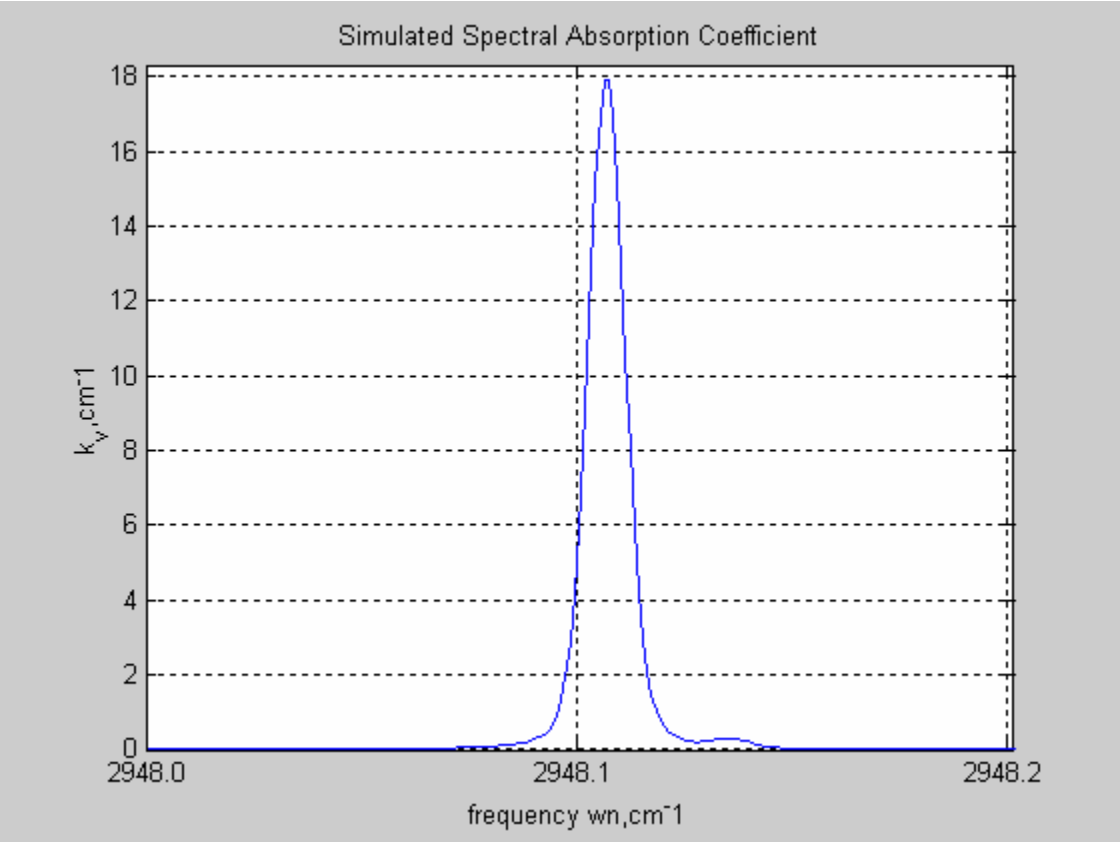

Figure 3.12. Methane Transition. The transition at 3392 nm (2948.1 cm^{-1}) was probed in this study.

3.2.2. Measurement Sensitivity. The basic means for errors entering the methane absorption measurement are the same as for the TDLAS measurements. In this case, the spectroscopic parameters are well known because a room-temperature transition is used. Also, the measurement is taken in an area where the flow is well mixed, so errors arising from flowfield non-uniformity are reduced in the acoustic-forcing tests. Tests where equivalence ratio is forced may result in non-uniformities. Narrow bandwidth interference filters were placed on the detectors to block the measurement of undesired IR emissions. Since a separate reference detector was used, errors presented from baseline determination are eliminated.

3.2.3. Experimental Hardware. The hardware for methane absorption measurements includes an Infrared Helium-Neon laser, optics, and detectors (Figure 3.13). The laser (Particle Measurement Systems LHIR-0100-339) operates at 3392 nm with a nominal power of 1.8 mW. Unlike the diode lasers, the He-Ne laser operates at only one wavelength and power. First, part of the beam is split off using a quartz window as a beamsplitter and sent to an InAs detector (Electro-Optical Systems IA-010-H) to monitor power fluctuations. The detectors are protected from extraneous emission by narrow-bandwidth filters. The main beam is collimated with a long-focal length lens (Oriel). In the laminar burner, sapphire windows are fused onto the ends of 5/8-inch stainless steel tubes to allow optical access upstream of the flame, as seen in Figure 3.14. The tubes can be moved to adjust the path length. In the turbulent combustor, threaded tubes hold the sapphire windows in place, as seen in Figure 3.15. Since the emission of the IR He-Ne corresponds to a very strong methane transition, the path length is limited to 2-3 cm in order to maintain adequate signal to noise ratios. After the beam is sent through the combustor, it is sent to a second InAs detector.

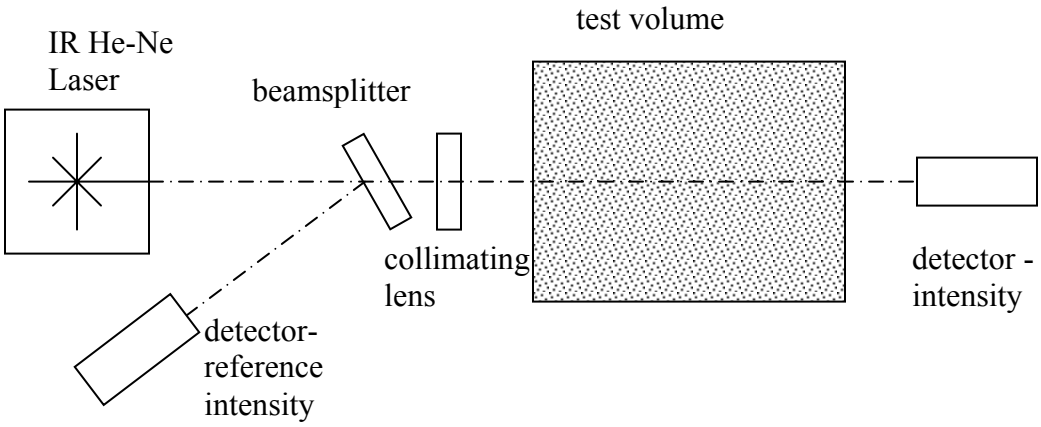

Figure 3.13. Methane Absorption Experimental Setup. The measurement is taken upstream of the flame.

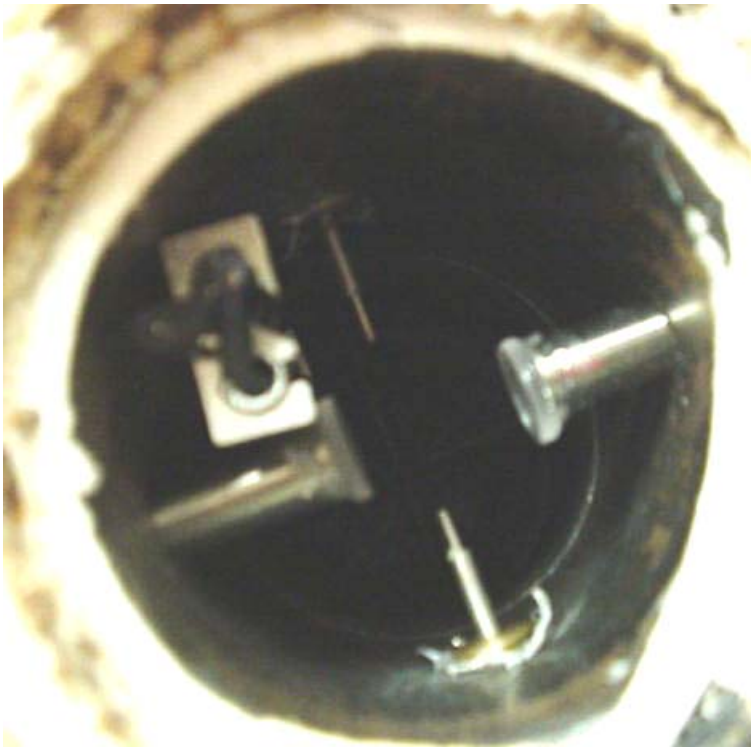

Figure 3.14. Window Assembly – Laminar Burner. Windows are mounted on tubes to adjust the pathlength.

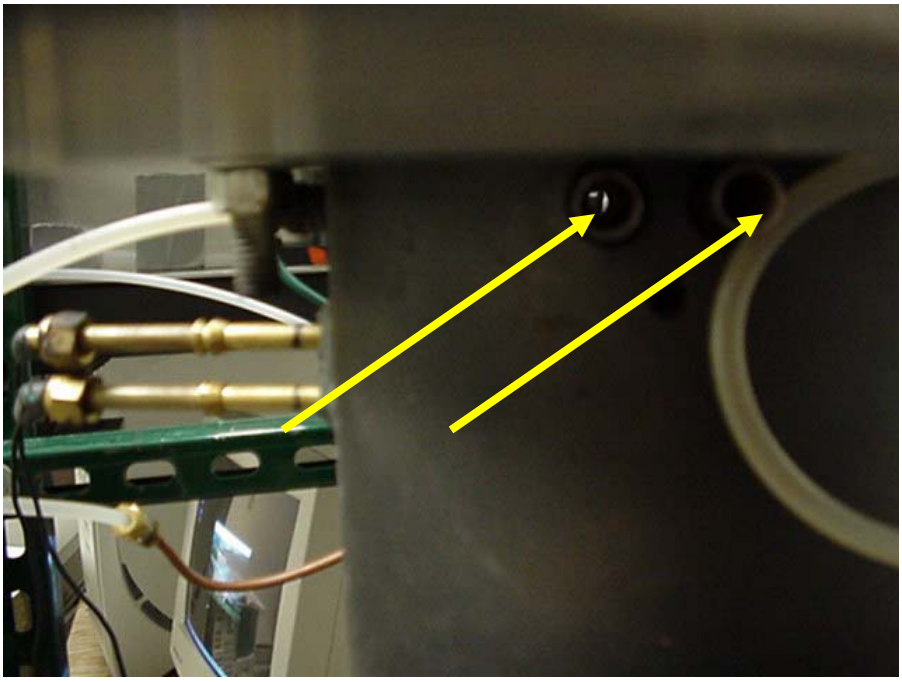

Figure 3.15. Window Assembly – Turbulent Combustor. Threaded tubes hold sapphire windows in place.

3.3 Hydroxyl Radical Chemiluminescence

Hydroxyl radical (OH*) chemiluminescence was used as an indicator of chemical heat release rate, or reaction rate, in this study.

3.3.1. Species Candidates. Many chemiluminescent species have been used as indicators of heat release rate, including CH*, CO2*, C2*, and OH* (where the * indicates an excited radical). OH* was chosen for many reasons. First, it is a simple molecule, and thus exhibits a relatively finite spectrum. The levels of OH* observed in a flame are far greater than the levels predicted by equilibrium chemistry at the flame temperature. This means the OH* is produced as an intermediate step in combustion reactions, and should be a good indicator of chemical reaction rate. Ludwig Haber confirmed this hypothesis for the static case. The reaction path $HCO + O \rightarrow CO + OH^*$ was proposed in lieu of the traditionally accepted reaction $CH + O_2 \rightarrow CO + OH^*$. An experimental and computational investigation confirmed OH* is an accurate indicator of chemical heat release rate [3]. Current work in the VACCG focuses on confirming the relationship for the dynamic case.

3.3.2. Experimental Hardware – Laminar Burner. The chemiluminescence experimental setup includes optics, fiber optic cables, a monochrometer, and a photomultiplier tube. The receiving optics are shown in Figure 3.16. The details of the system are given by [3]. All optics are fused-silica to ensure transmission (98%) of ultraviolet light. Two 25.4-mm fused silica lenses are used to collect the light from an area with a diameter 1.2 times the diameter of the flame and focus it onto the fiber optic cable. A fiber optic positioning module (Newport) couples with the SMA termination on the fiber. The optical fiber used is 1-mm in diameter with a fused-silica core and 0.48 numerical aperture, with SMA terminations. The fiber optic cable carries the light to a 0.5 m Ebert Monochrometer (Jarrell Ash 82-020) with a 400 nm diffraction grating set to 309 nm for OH* chemiluminescence. The light flux is converted to an electric current flux via a photomultiplier tube (Hamamatsu R995), powered via a high-voltage power source.

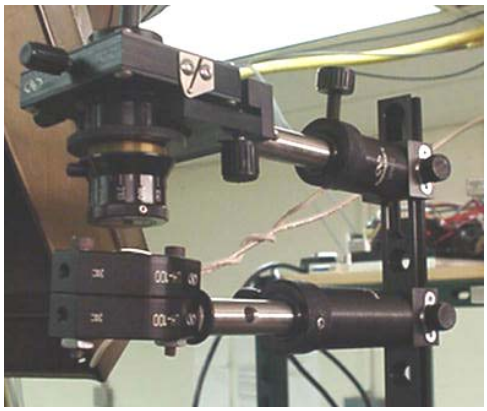

Figure 3.16. OH* Chemiluminescence Receiving Optics – Laminar Burner. Fiber optics carried light to a monochrometer.

3.3.3. Experimental Hardware – Turbulent Combustor. The chemiluminescence system for the turbulent combustor uses an optical filter (307FS10-50 Andover Corp.) to select the light emission due to hydroxyl radical (OH*) chemiluminescence, as seen in Figure 3.17. The filter has a peak transmittance of 15.04% at 307.81 nm, with a full width at half the maximum of 19.08 nm. A fused-silica lens, 50.8 mm diameter and 75 mm focal length, allowed the collection system to focus on the reaction zone of the combustor. The optics were mounted directly to a Hamamatsu R955 photomultiplier tube. A high-voltage power supply provided 890 V to the photomultiplier tube.

Figure 3.17. OH* Chemiluminescence Receiving Optics – Turbulent Combustor. The turbulent combustor used a lens and filter system.

3.4 Velocity Sensor

The velocity perturbation must be known upstream of the flame in order to measure frequency responses of flame dynamics. Based on the two-microphone technique [4, 5], two ultra-miniature tie-clip microphones (Radio Shack, model number 33-3003) are spaced 55 mm apart using a spacer as seen in Figure 3.18 in the laminar burner. In the turbulent combustor, holes 19 mm apart allow microphones to be mounted directly upstream of the swirler as seen in Figure 3.19. An analog circuit serves to condition the signal and simulate the integral form of the momentum equation with no body forces, equation 3.4. The specifics of the probe are given in [6].

$$u'(t) = \int_0^T \frac{1}{\rho} \frac{\partial p'}{\partial x} dt \tag{3.4}$$

Figure 3.18. Velocity Sensor used in the Laminar Burner. The sensor is located directly upstream of the honeycomb.

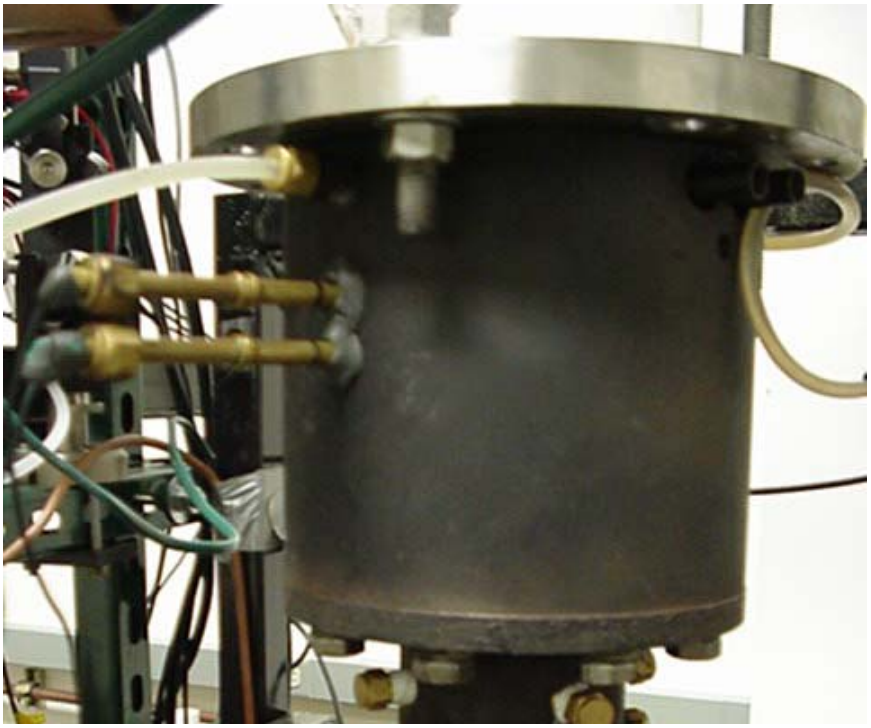

Figure 3.19. Velocity Sensor used in the Turbulent Combustor. The sensor is located upstream of the swirler.

Figure 3.20 shows the frequency response and coherence between the two microphones used in the velocity probes used in this study. Microphones were tested and two microphones with similar frequency responses were chosen. The microphones used in the laminar burner varied less than 1 dB in magnitude and 5 degrees in phase.

To determine the bandwidth over which the velocity probe output was valid, the velocity frequency response was measured for the frequency range of interest. The velocity probe used in the laminar burner exhibited a coherence above 0.9 for the frequency range 30-510 Hz, and 540-2000 Hz, as seen in Figure 3.21. It is evident that there is a velocity node at the plane of measurement at 520 Hz in the laminar rig. Thus, care must be taken when exciting the flame near 520 Hz to provide an adequate velocity perturbation to the flame. The velocity probe used in the turbulent burner exhibits coherence above 0.7 for the frequency range 40-150 Hz and 200-600 Hz, as seen in Figure 3.18. Similarly to the laminar burner, there is a velocity node at 160 Hz. Since the transmission of an acoustic wave changes with frequency, as shown in Figure 3.21, the amplitude of the forcing (voltage to the speaker) must be changed with frequency when measuring the frequency response of the flame to insure an adequate velocity perturbation reaches the flame. This will be further discussed in the experimental procedure sections (Section 4.2 and 5.2).

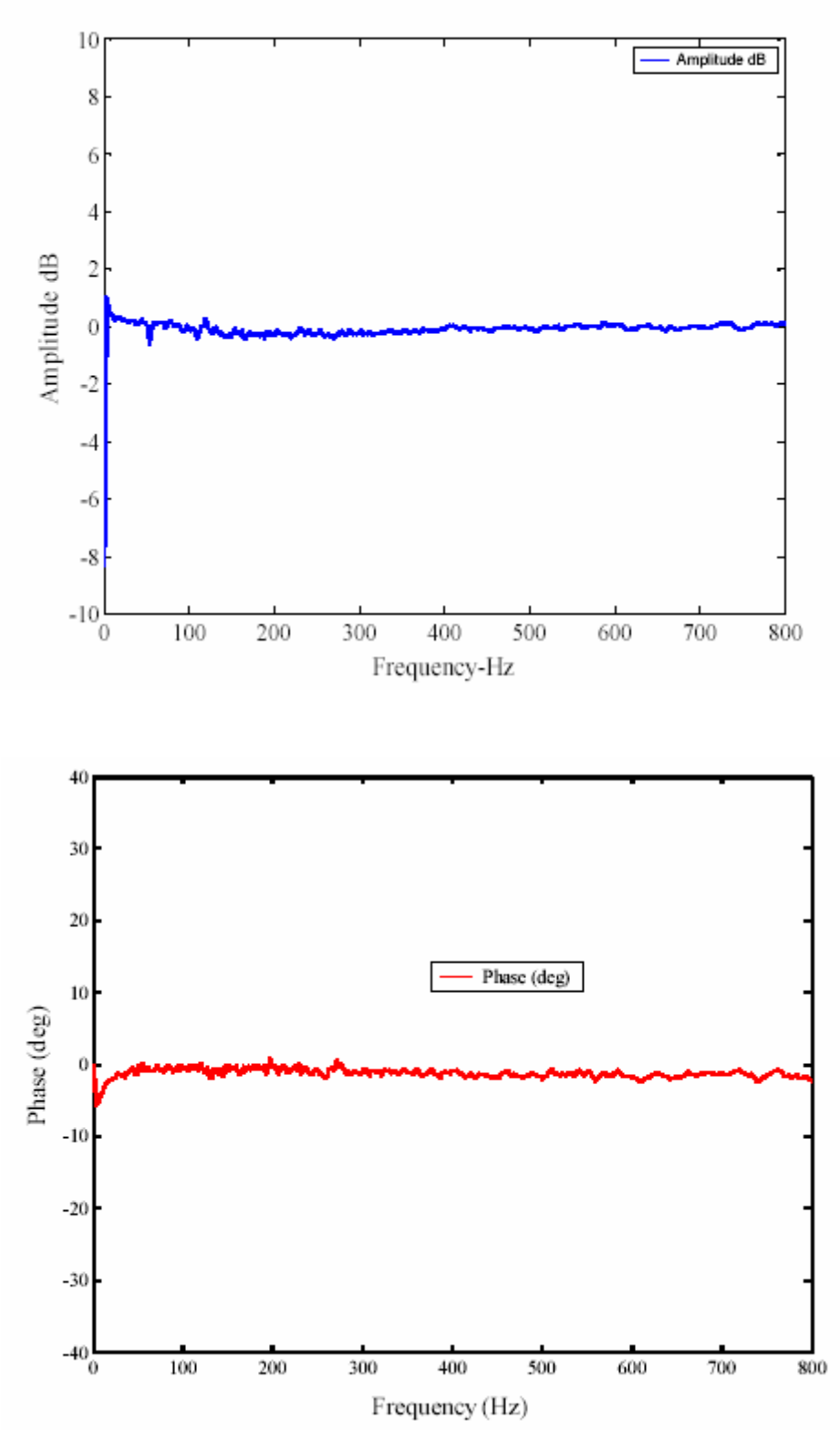

Figure 3.20. Frequency Response and Coherence between Microphones. The responses of the two microphones matches well. Plots from [6].

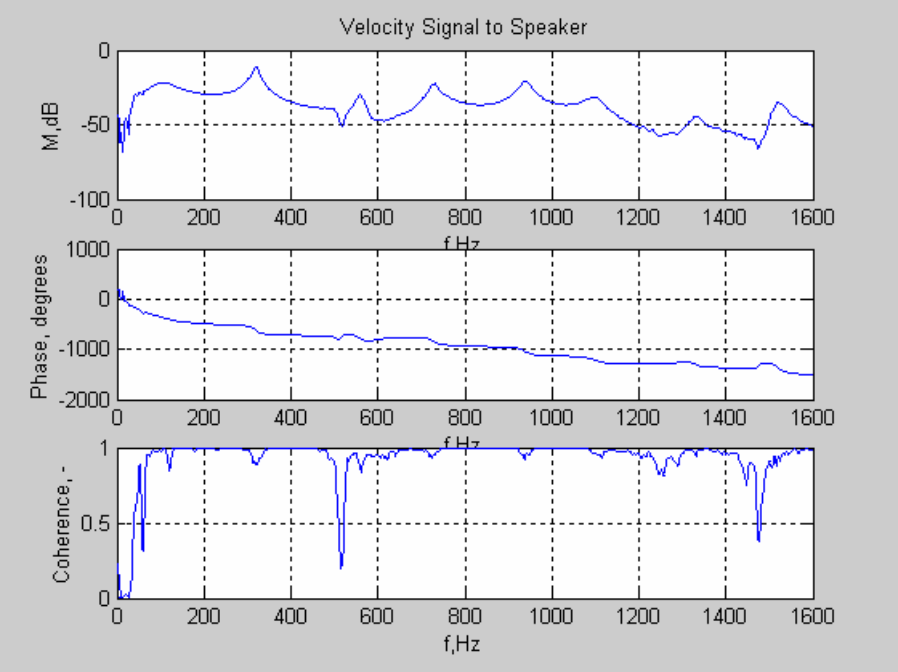

(a)

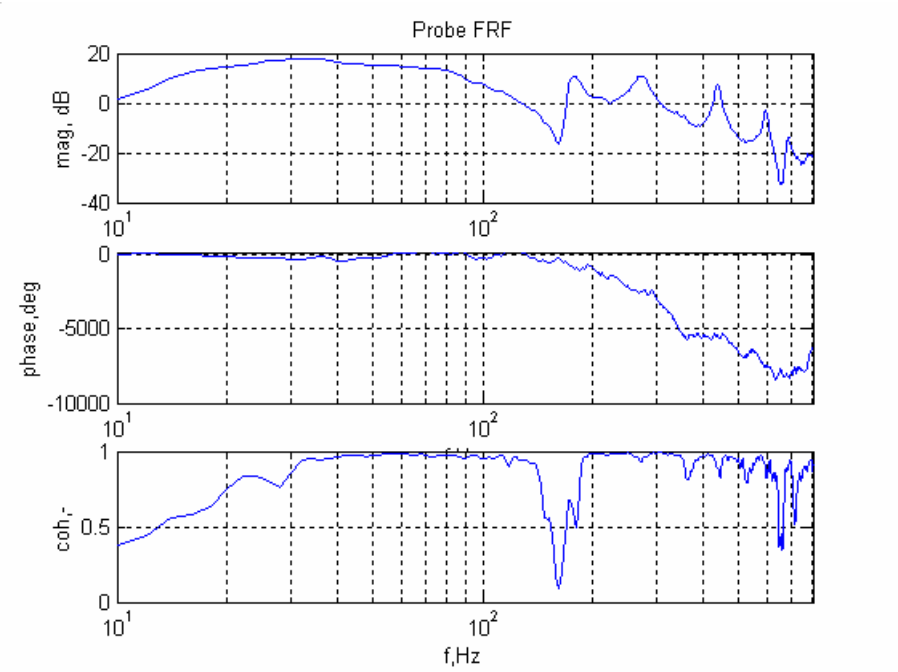

(b)

Figure 3.21. Velocity Frequency Response and Coherence. (a) laminar burner, (b) turbulent combustor.

It is necessary to calibrate the velocity probe signal, in Volts, to physical units. The velocity probe simulates the 1-D Euler equation,

$$u' = -\frac{1}{\rho}\int \frac{\partial p'}{\partial x} \cong -\frac{1}{\rho}\frac{(\Delta p)}{\Delta x} = \left[\frac{m}{s^2}\right]$$

where

$$\Delta p = V_d \cdot \left(\frac{S_m}{S_a}\right) = [Pa]$$

$$\Delta x = length\ between\ microphones = [m].$$

$$\rho = density = \left[\frac{kg}{m^3}\right]$$

The sensitivity of the microphone, S_m, is measured by comparing the output of the microphone used with a calibrated B&K microphone. The sensitivity of the microphones used in this study is 100 Pa/Vmic. The sensitivity of the amplifier in the circuit, S_a, is the gain of the circuit. The frequency response of the circuit is shown in Figure 3.22. The sensitivity is taken as the DC value. Using these values, the calibration for the velocity probe becomes

$$u'_{turb} = 9.915 \cdot V_d$$
$$u'_{lam} = 0.1403 \cdot V_d$$

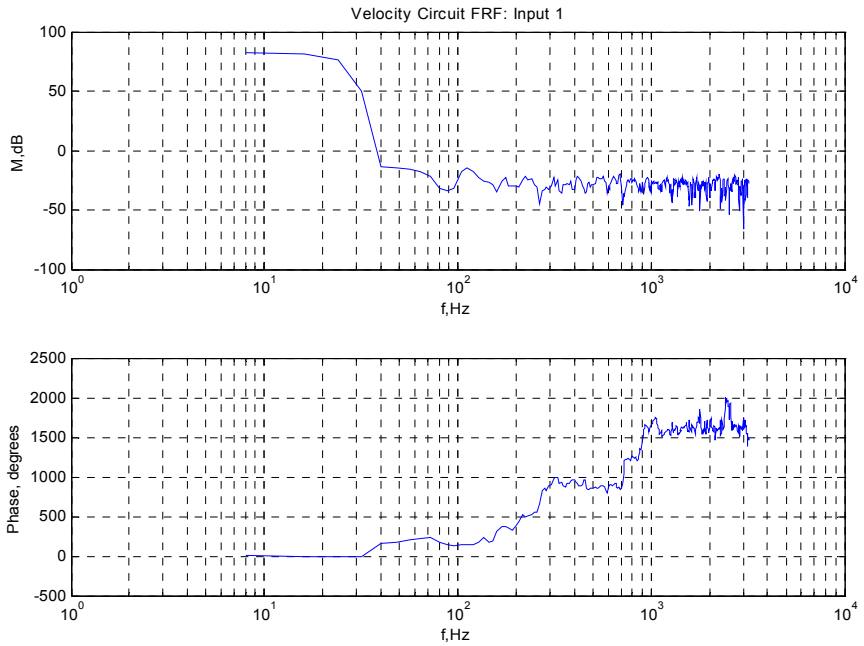

(a) circuit for laminar burner

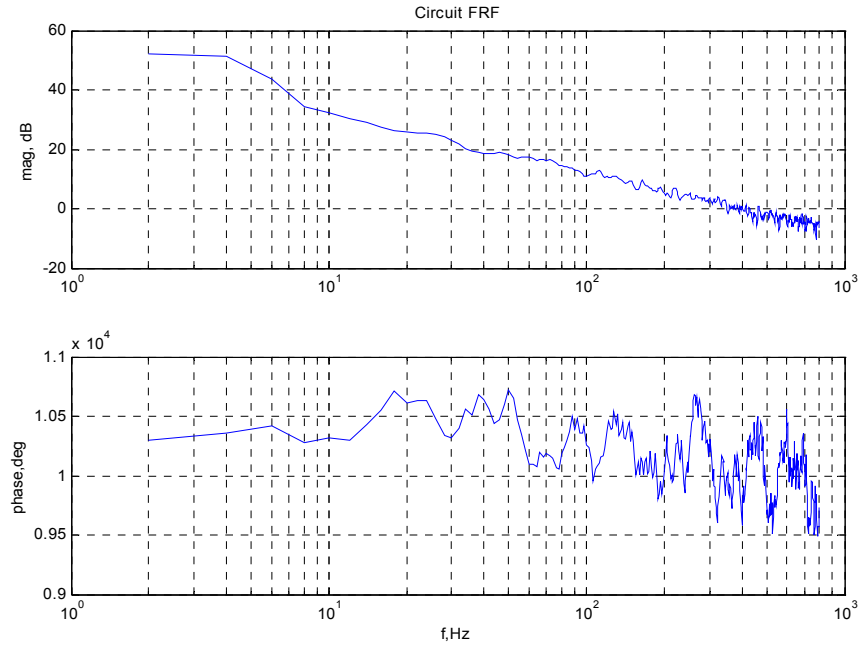

(b) circuit for turbulent burner

Figure 3.22. Circuit Frequency Response Function. The response of the circuit to random noise input.

3.5 Laminar, Flat-Flame Burner

3.5.1. Design. The laminar, flat-flame burner used in this study was designed specifically for flame dynamics studies. The burner will be described briefly here as the details of the design can be found in the doctoral thesis of Vivek Khanna [7]. In order to observe the effect of velocity and equivalence ratio perturbations on the unsteady heat release of the flame, the combustor must be stable. In other words, the Rayleigh Criterion must not be satisfied so that heat release oscillations do not feedback into the unsteady pressure of the combustor, causing instabilities. An attempt was also made to make the results of the flat-flame burner experiments relevant to turbulent, swirl-stabilized flames in gas turbines. The flame temperature was kept close to the flame temperatures in full-scale gas turbines by using a ceramic honeycomb as a flame holder. The honeycomb served to transfer energy to the incoming flow, increasing the velocity of the flow into the flame and allowing higher flame temperatures.

3.5.2. Apparatus. A schematic and photograph of the laminar, flat-flame burner is shown in Figure 3.23. The premixed charge enters the 100-mm diameter plenum through ¼" tubes with equi-spaced, 1/64" diameter holes. The injectors allow for even distribution of the flow as well as high acoustic impedance to decouple upstream acoustics. After the plenum, the flow is accelerated through a bell reducer(100mm to 65 mm) to ensure radial homogeneity as well as purely axial flow. The flame is stabilized on a ceramic honeycomb, 18 mm thick and 68 mm in diameter. The flame is protected from ambient flows using a 75 mm diameter quartz tube.

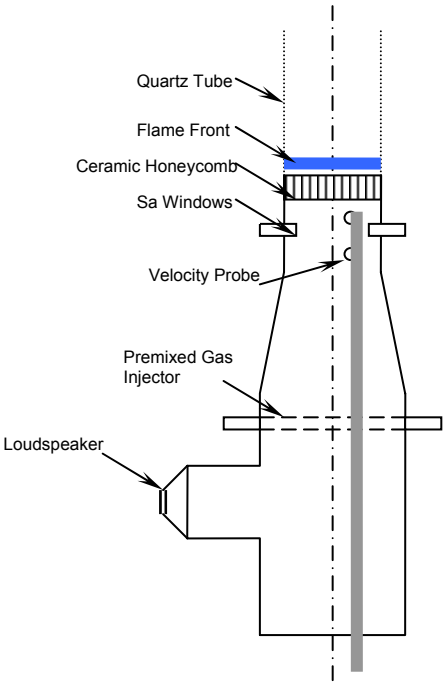

(a)

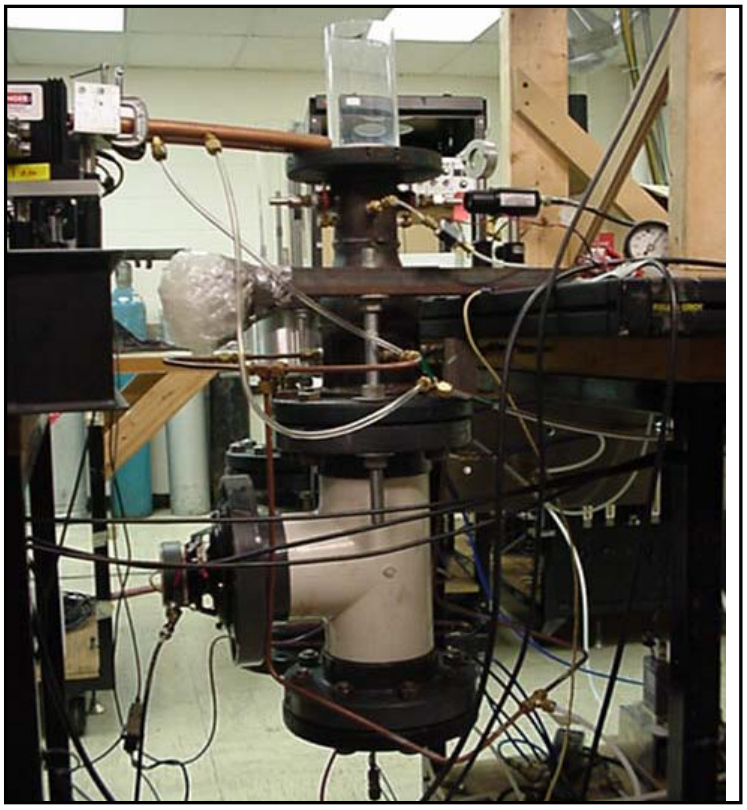

(b)

Figure 3.23. Laminar Flat-Flame Burner. The stable burner was used to study laminar flame dynamics.

A loudspeaker is attached to the side branch of the plenum to force perturbations in velocity, or mass flow rate. Care was taken to impart the velocity fluctuations far enough downstream of the flame to ensure 1-D planar waves reach the flame, free of near-field effects of the loudspeaker. The velocity sensor, described in the preceding section, is located directly upstream of the honeycomb to measure velocity fluctuations.

To impart fluctuations in equivalence ratio, another injector tube was added 5 cm upstream of the honeycomb. A secondary fuel flow is sent through a Matrix 851 fast-solenoid valve with a bandwidth of 500 Hz. The window assembly that allows access for equivalence ratio fluctuation measurements, described in Section 3.2, is located 1.5 cm upstream of the honeycomb.

3.6 Turbulent, Swirl-Stabilized Combustor

3.6.1. Design. The turbulent, swirl-stabilized combustor was designed to simulate the combustion chamber of a typical gas turbine. Details of the design and apparatus can be found in the doctoral thesis of Vivek Khanna [7]. Many current gas turbine combustors use swirl-stabilization. The flame is hydrodynamically-stabilized on vortices resulting from the combination of swirling flow and a sudden expansion.

3.6.2. Apparatus. The turbulent, swirl-stabilized combustor is shown in Figure 3.24. The main air and fuel mixture enters through the axial air inlets. A user-defined fraction of the air/fuel mixture can enter through the tangential air inlets, thereby modifying the swirl. The tangential air inlets were not used in this study. The combustor was modified to allow for static swirlers and optical access for equivalence ratio fluctuation measurements, as seen in Figure 3.25. Radial fuel injection ports can be used for secondary fuel. A sudden expansion, along with the swirling flow, stabilizes the flame in the 125mm-diameter Quartz combustor section. A plate downstream of the combustor section allows the addition of an orifice to pressurize the rig up to 150 psig. A two-microphone probe, as described in Section 3.5, is used to measure velocity fluctuations.

Velocity fluctuations are imparted via a 130mm-diameter speaker mounted on a side branch.

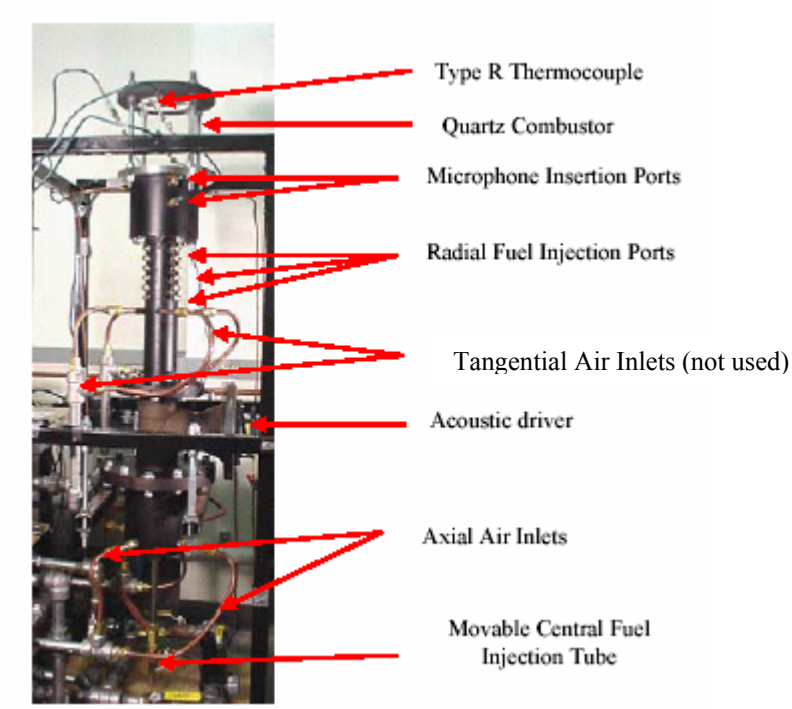

Figure 3.24. Turbulent, Swirl-Stabilized Combustor [7]. Swirl-Stabilized combustors are used in many current gas turbines.

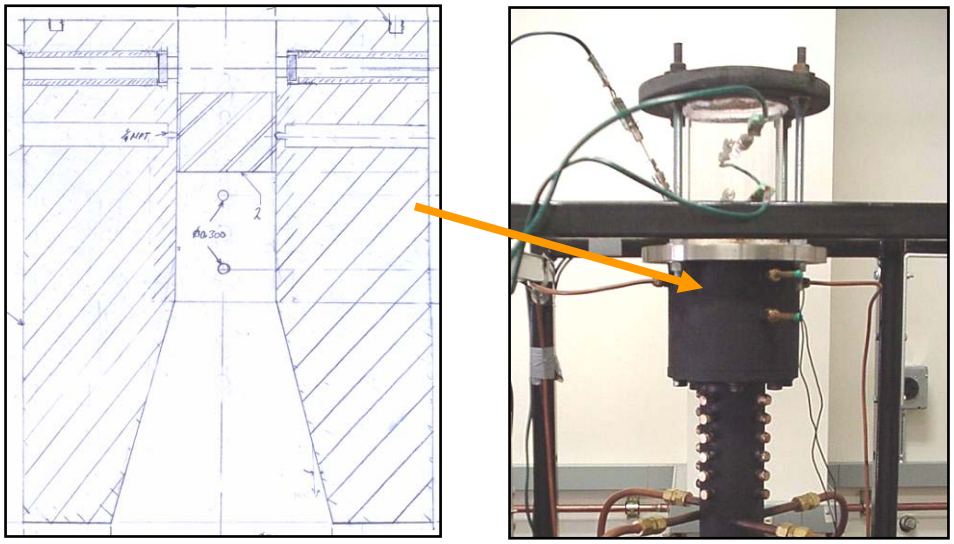

Figure 3.25. Rig Modifications. The turbulent rig was modified to allow for static swirlers and optical access to measure equivalence ratio fluctuations.

3.7 Data Acquisition System

A PC-based data acquisition system was used to record data for flame dynamics experiments. The system consists of an 800 MHz personal computer with a 16-bit, 100,000 samples per second, data acquisition card (National Instruments PCI-MIO-16XE-10). National Instruments SCXI modules perform the signal conditioning. First, the signals go through an 8^{th} order Bessel low-pass filter for anti-aliasing (SCXI-1141). The anti-aliasing filter also has a software-selectable gain up to 100. Next, the signals are sent to a simultaneous sample-hold card (SCXI-1140) with an optional gain of up to 800. The PCI-MIO-16XE-10 card also provided two analog outputs. The data acquisition is controlled through Labview ©. Codes (flame_dynamics.vi, flame_dynamics_turb_r1.vi) were written to modulate the diodes to take reference absorption profiles, perform the sine dwell and collect data, and record test parameters. Post processing (i.e. frequency response functions, power spectra, etc.) was completed using Matlab ©.

Bibliography

1. Furlong, E.R., *Diode-laser absorption spectroscopy applied for the active control of combustion*, in *Mechanical Engineering*. 1998, Stanford University: Stanford, CA.
2. Rothman, L.S., et al., *The HITRAN molecular spectroscopic database: edition of 2000 including updates through 2001.* Journal of Quantitative Spectroscopy & Radiative Transfer, 2003.
3. Haber, L., *The relationship between OH chemiluminescence and chemical reaction rate in laminar premixed combustion*, in *Mechanical Engineering*. 2000, Virginia Tech: Blacksburg, VA.
4. Waser, M.P. and M.J. Crocker, *Introductionto the two-microphone cross-spectral method of determining sound intensity.* Noise Control Engineering Journal, 1984. **May-June**: p. 76-85.
5. Seybert, A.F. and D.F. Ross, *Experimental determination of acoustic properties using a two-microphone random-excitation technique.* Journal of the Acoustical Society of America, 1976. **61**(5): p. 1362-1370.
6. Khanna, V.K., et al., *Dynamic analysis of burner stabilized flames part 1: laminar premixed flames.* American Flame Research Committee (AFRC) International Symposium, 2000.

7. Khanna, V., *A study of the dynamics of laminar and turbulent fully and partially premixed flames*, in *Mechanical Engineering*. 2001, Virginia Tech: Blacksburg, VA.